https://doi.org/10.5194/egusphere-2024-2181
Preprint. Discussion started: 19 July 2024

Inverse Differential Equation Modeling of ENSO Prediction Based on Memory Kernel Functions

Shiquan Wan[1,2], Hongjia Lei[2], Lingzhi Zhang[2], Xintong Zhao[3], Shasha Xu[1], Mengsheng Qin[1], Yuan Cheng[1], Qianrong Ma[2*]

[1]Jiangsu Yangzhou Meteorological Bureau, Yangzhou, 225009, China
[2]College of Physical Science and Technology, Yangzhou University, Yangzhou, 225012, China
[3]China Meteorological Administration Aviation Weather Service Key Laboratory, Beijing, 100086, China

Correspondence to: Qianrong Ma (maqianron_g@163.com)

Abstract. The ENSO system is a complex climate pattern that is crucial in global climate systems and plays a key role in climate prediction. Both statistical methods and numerical models have been dedicated to achieving accurate predictions of ENSO variations; however, there is still a considerable gap in practical applications. Therefore, we proposed a memory kernel function-based approach to solve the inverse problem of ENSO time-varying systems. We attempted to establish differential equations by constructing memory vectors composed of multiple initial values to describe the evolutionary characteristics of this complex system. Unlike traditional inverse problem-solving methods, our research scheme delved into the inherent properties exhibited by ENSO, such as memory and periodicity, and embedded these properties as specific targets in differential equations. By leveraging the flexibility of evolutionary algorithms to solve mathematical problems, we achieved targeted modeling of the ENSO system. The results demonstrate that this scheme overcomes the limitations of traditional differential equations with a single initial value and extends these equations to memory vector equations based on multiple initial values. This not only enhances our ability to describe the evolutionary laws of complex systems but also improves the timeliness and reliability of ENSO predictions, achieving encouraging results.

1 Introduction

The urgency to predict short-term climate change with precision is critical given the increasing frequency and intensity of extreme weather events. Accurate climate predictions play a vital role in formulating disaster-prevention and mitigation policies (Hwang et al., 2021; Usman, 2017). As one of the countries most severely affected by meteorological disasters, China experiences approximately 55% of the deaths and 87% of the direct economic losses caused by natural hazards worldwide. Furthermore, if weather-related secondary geological

https://doi.org/10.5194/egusphere-2024-2181
Preprint. Discussion started: 19 July 2024

disasters occur, these figures will increase to 81% and 89%, respectively (Wu et al., 2014). Therefore, improving the accuracy of short-term climate predictions has considerable socioeconomic and scientific importance (Guan et al., 2015).

Climate models have become sophisticated and prevalent tools for simulating the interactions between the atmosphere, oceans, land surface, and ice (Eyring et al., 2019; Masson and Knutti, 2011). Based on physical principles, dynamic models use equations that describe atmospheric and oceanic processes (Palmer, 2001). These models require substantial computational resources and detailed initial conditions, making them powerful for long-term projections but often less effective for short-term predictions involving rapid changes and smaller scales (Alizadeh, 2022). Additionally, statistical models rely on historical data, are generally less computationally intensive, and can be useful for short-term forecasts (Sunyer et al., 2012). However, they are typically restricted to historical data and have a limited ability to predict unprecedented or highly variable events (Kjellström et al., 2010). Therefore, combining the strengths of dynamic and statistical approaches has emerged as a promising strategy for enhancing short-term climate prediction (Mittal et al., 2015; Feng et al., 2020). These advancements have substantially improved short-term rainfall and temperature predictions in eastern China (Wei, 2011; Tian et al., 2015; Zhang et al., 2018).

When utilizing current modeling capabilities and statistical theories, making substantial improvements in prediction accuracy through external optimization alone and addressing the biases in climate predictions at small spatial scales remain challenging in the short term. Numerical climate predictions inevitably have considerable biases that are challenging to address (Eyring et al., 2019). Thus, relying solely on numerical model outputs to address local climate prediction issues in different regions remains unsatisfactory. Statistical methods have been used for more than half a century (Sedki et al., 2009; Feng et al., 2019). These methods rely on the assumption that time series are stationary, making them less suitable for dealing with nonstationary nonlinear problems (Mirikitani and Nikolaev, 2010; He et al., 2012). However, climatic evolution processes often exhibit nonlinear and nonstationary characteristics. Ma et al. (2023) emphasized that the differential prediction method based on time series is nonlinear, combining the advantages of numerical models and the convenience of traditional statistical methods. This method has the functionality of continuous multi-step iterative prediction, like numerical models, and it can handle complex relationships between variables.

Therefore, our research was based on the memory characteristics of the climate system and addressed the limitations of a single initial value in numerical model methods. Specifically,

https://doi.org/10.5194/egusphere-2024-2181
Preprint. Discussion started: 19 July 2024

differential equation modeling of multi-initial memory kernel functions (MIMKFs) has emerged as a novel approach with considerable potential for improving the accuracy of short-term climate forecasts. The MIMKFs are a sophisticated class of differential equations that incorporate multiple initial conditions and memory effects into their framework (Ma et al., 2023). These equations were designed to capture the dynamic behavior of climate systems, where the future state depends not only on the present conditions but also on a series of past states. Furthermore, MIMKFs are particularly suitable for modeling complex time-dependent systems (Wan et al., 2012). This multi-initial approach mitigates the limitations of traditional single-initial-condition models, which may overlook large variations, leading to less reliable predictions (Feng et al., 2001). Moreover, the self-memory aspect of these differential equations allows for the incorporation of past climatic events and trends, enhancing the ability of the models to predict future states. Targeted modeling can utilize limited resources and data more effectively to improve modeling and prediction (Olivetti and Messori, 2023). This is particularly crucial for short-term climate predictions, where recent weather patterns and anomalies greatly influence future conditions (Dong et al., 2004; Chen et al., 2009). Thus, by leveraging the strengths of MIMKFs and targeted modeling, predictive tools can provide timely and accurate forecasts, which are essential for disaster preparedness and mitigation efforts.

For complex climate systems, the main challenge in prediction is the complexity of the constituent components of the system. The system evolution process typically includes not only major cycles but also various high-frequency disturbance components (Feng et al., 2020; Wang et al., 2021). For example, sea surface temperature (SST) is a complex composite signal formed by the superposition of multiple cycles. Chen et al. (2004) used a hybrid statistical–dynamic modeling system and SST data to discuss the relative role of atmospheric noise and the initial ocean state in determining the predictability of the El Niño–Southern Oscillation (ENSO) system. Lima et al. (2009) developed a two-stage statistical ENSO forecasting model to understand the possible sources of longer-range ENSO predictability. Statistical models, such as principal component analysis, have been widely used to capture the main modes of ENSO and to reduce the dimensionality of the predictors in forecasting (Drosdowsky, 2006; Lu et al., 2017). However, most statistical models assume that the embedding space is a linear subspace of the original data.

Therefore, in this study, we aimed to produce improved statistical forecasts of ENSO as represented by the Niño3.4 index via the nonlinear MIMKFs method. To this end, we first studied the periodicity of the SST time series, performed wavelet transforms to obtain two-

https://doi.org/10.5194/egusphere-2024-2181
Preprint. Discussion started: 19 July 2024

dimensional time-frequency variation plots, extracted specific periods, and laid the groundwork for constructing periodic memory kernel functions (MKFs). Second, we conducted an inertial memory analysis of non-periodic components to seek theoretical bases for constructing inertial MKFs. Finally, based on the two memory principles, the basic differential forms of the MKFs were predefined in the modeling process, dynamic system target modeling of SST was conducted, and the actual performance of the MIMKFs' predictability of ENSO was examined.

2 Material and Methods

2.1 Data

We used the indices for ENSO, particularly the Niño3.4 index (Reynolds and Smith, 1994) provided by the National Oceanic and Atmospheric Administration. The data are available at: https://www.esrl.noaa.gov/psd/gcos_wgsp/Timeseries/Nino34/.

2.2 Inverse differential equation modeling of MKFs

The classical approach to solving inverse problems, which relies on simplified differential equations with a single initial value, is inadequate for characterizing complex climate systems. Inverting complex climate systems requires the construction of sophisticated differential equations, thereby demanding advanced parameter estimation techniques. To capture the complex characteristics of ENSO, we proposed using MKFs based on multiple initial values and employed flexible evolutionary algorithms for parameter estimation.

We assumed that the dynamic differential equation of the ENSO system was:

$$\frac{dx}{dt} = F\,(x, p, q, t) \tag{1}$$

Where $x \in R^n$ represents the state vector of the system; $p, q \in R^n$ denotes unknown parameter vectors; t is time; and F represents an unknown vector function. Using inverse differential equation modeling, the characteristics of ENSO and the related parameter p can be expressed using observational data $y(t_i)$ (where t_i denotes the observation time points, $i = 1, 2, \ldots, N$). On assuming that F possesses a specific structure or form that includes the undetermined parameter p, the function F_a can be defined as follows:

$$F_a\,(\mathrm{x}, \mathrm{p}, \mathrm{t}) = \mathrm{m}(\mathrm{x}, \mathrm{p}, \mathrm{t}) + \mathrm{f}(\mathrm{q}, \mathrm{t}) \tag{2}$$

https://doi.org/10.5194/egusphere-2024-2181
Preprint. Discussion started: 19 July 2024

Where p and q are unknown parameters and their values are estimated using evolutionary algorithms. Notably, functions m and f contain self-memory information (MKFs or basis functions), and their specific forms are dynamically determined using evolutionary algorithms.

To estimate the undetermined parameters p and q and the functions m and f, an error function $E(m, f, p, q)$ that measures the discrepancy between the assumed model and observation must be constructed. Then, the error function can be defined using the least-squares method as follows:

$$E(\mathrm{m}, \mathrm{f}, \mathrm{p}, \mathrm{q}) = \sum \| x(t_i) - y(t_i) \|^2 \quad (3)$$

Where $x(t_i)$ is the simulated state vector obtained from the assumed model F_a through numerical integration using the Runge–Kutta method. Subsequently, we employed a genetic algorithm to minimize the error function, thereby estimating the parameters p and q and the functions m and f. We generated an initial population containing multiple parameter vectors for p and q and the gene expressions of functions m and f. For each parameter vector (p_j, q_j, m_j, f_j) in the population, we computed the corresponding simulated state vector $x(t_i)$ and calculated the error function. The fitness of each parameter vector was evaluated based on the values of $\mathrm{E}(p_j, q_j, m_j, f_j)$. Furthermore, a subset of the parameter vectors was selected based on their fitness for crossover and mutation. Parts of the two parameter vectors were combined through crossover operations, and genes were randomly altered through mutation operations to generate new parameter vectors. This process was repeated until the parameter vector with the highest fitness was produced.

3 Results

3.1 Analysis of SST memory patterns

Analysis of SST memory patterns involve more than simply randomly distributing the initial value vector for evolutionary modeling. It is also necessary to study the memory patterns of the target system prior to modeling. Herein, the monthly-scale SST corresponding to Niño3.4was chosen as the research subject, with SST anomaly data available from January 1951 to July 2022, spanning approximately 860 months. Typically, complex systems exhibit memory characteristics through two main approaches: periodic oscillations, referred to as "periodic memory" and inertial motion, termed "inertial memory". Initially, a periodic analysis was conducted on SST data to determine the characteristic parameters for constructing specific

https://doi.org/10.5194/egusphere-2024-2181
Preprint. Discussion started: 19 July 2024

MKFs. We employed wavelet analysis to obtain a time-frequency plot of monthly SST anomalies (Fig. 1).

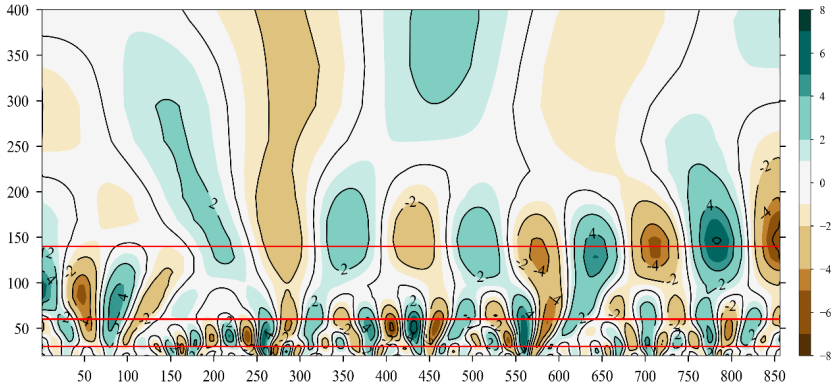

Figure 1: Time-frequency plot of wavelet transform for SST anomaly sequence.

As shown in Fig. 1, the SST exhibits predominant cycles ranging from large to small scales, primarily at 140, 60, and 30 months. When converted to annual scales, these correspond to distinct cycles of approximately 11 years, noticeable cycles of approximately 5 years, and less-apparent cycles of approximately 2.5 years. These cycles appear to be relatively stable after the 210th month, corresponding to the period from 1969 to 2022. The remaining components represent less-apparent cycles characterized by high-frequency oscillations, which are considered to be inertial motions.

https://doi.org/10.5194/egusphere-2024-2181
Preprint. Discussion started: 19 July 2024

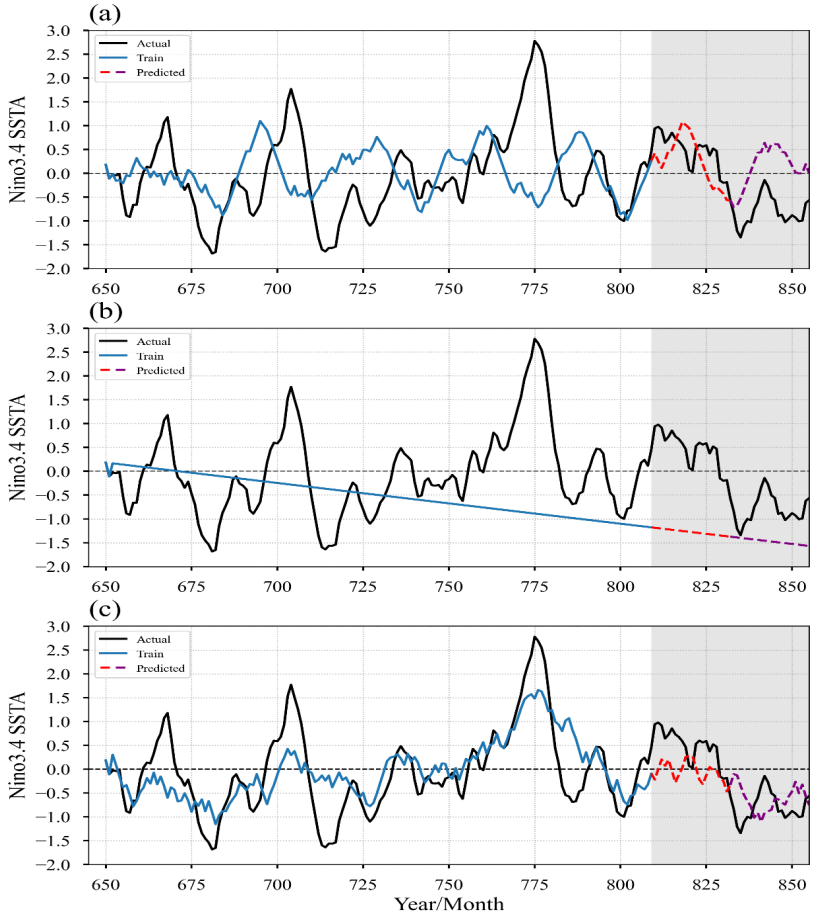

Figure 2: (a) Integral curve of the memory kernel function (MKF) (t, sst), (b) high-frequency component, and (c) integral curve of the SST modeling based on MKFs. The black line represents observed values, the blue line indicates fitting, and other colors represent the testing interval.

Based on the time-frequency plot of the wavelet analysis, the earlier periods of SST exhibit relatively complex periodic patterns. Therefore, it was chosen to model the later observational SST data. The training dataset consisted of 180 months (sample range: 650–838, from April 2005 to December 2018), while the testing dataset comprised 26 months (830–856, from January 2019 to July 2022). The specific expression for the $MKF(\sin t, X)$ obtained from evolutionary modeling is as follows:

$$MKF(t, sst) = 24.118\, sin\left(\frac{2\pi t}{60} + \frac{2945.3}{sst[-3]}\right) \quad (4)$$

https://doi.org/10.5194/egusphere-2024-2181
Preprint. Discussion started: 19 July 2024

where *t* represents time, *X* vector corresponds to the retrospective initial points of the SST, and sst[-3] denotes the observed value at the third previous time step of the current initial point sst[0]. It can be observed that the kernel function describes a memory signal with a period of 60 months and includes memory information from the SST of the third previous month (Fig. 2a). The high-frequency component f(t,X) is expressed as follows:

$$f(sst) = \frac{40.2}{sst[-5] + sst[-6] - sst[0] + 135.45} - 1.156 \quad (5)$$

Figure 2b shows that the higher-frequency component is described using information from SST observations of the fifth and sixth previous months. According to Fig. 2a and 2b, the kernel function and high-frequency component illustrate the characteristics and evolving trends of the SST periodic memory, respectively. Combining the periodicity of the former and the trend characteristics of the latter, the organically integrated training fitting and testing results are shown in Fig. 2c. Memory changes in SST have been described systemically. The ODE-MKF model achieved a correlation coefficient of 0.71 and a mean squared error of 0.63 for the training fitting, while for the testing part, the correlation was 0.68 with a mean squared error of 0.59. From the mathematical expression of the model, the ODE-MKF is relatively simple to calculate by embedding targeted kernel functions, yet it achieves a high accuracy in fitting SST data. Experiments conducted outside the sample have also indicated that the ODE-MKF can describe periodic changes in SST through periodic kernel functions, while the non-periodic component was described using a high-frequency component.

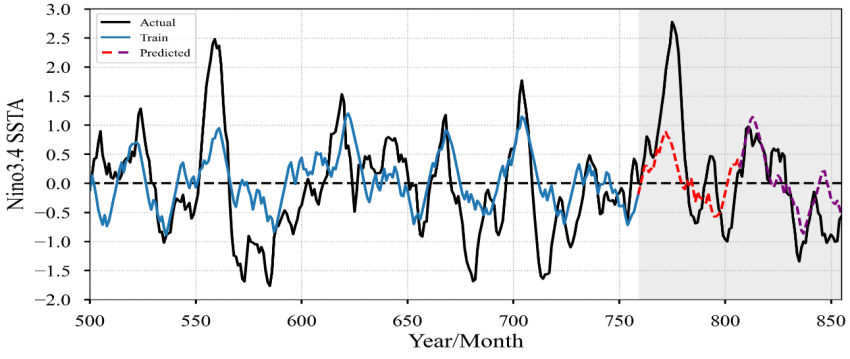

Figure 3: Integral curve of ODE-MKF for the long sequence.

Furthermore, by increasing the size of the training and testing samples, the difficulty of fitting can be enhanced. The inversion results for the setting [Model Parameter 2]: 260 months

https://doi.org/10.5194/egusphere-2024-2181
Preprint. Discussion started: 19 July 2024

of training samples (sample range: 500–760, from October 1992 to June 2014) and 95 months for testing the model (761–856, from July 2014 to July 2022) are shown in Fig. 3. Extending the model training interval increases the difficulty of fitting and describing the memory with kernel functions. As shown in Fig. 3, the blue line indicates a fitting correlation coefficient of 0.611 and mean squared error of 0.686. For the validation interval represented by the red part, the corresponding parameters were 0.63 and 0.693. The ODE-MKF performed well during the validation period and accurately predicted the main SST fluctuations. The reconstructed MKF involved two cycle ranges (140 and 30 months), indicating longer memory descriptions. The high-frequency component primarily comprised retrospective initial values that included certain nonlinear terms.

3.2 Inertial MKF

Random disturbances or processes in complex systems are not only difficult to predict but also tend to obscure the main periodic variations, thereby interfering with predictions. The transfer entropy method was employed as a diagnostic tool for assessing the inertial memory scales. In the following analysis, fluctuations in SST at the seasonal scale were examined to establish a theoretical basis for constructing the MKF. Using SST as an example, the inertial memory was analyzed using two methods.

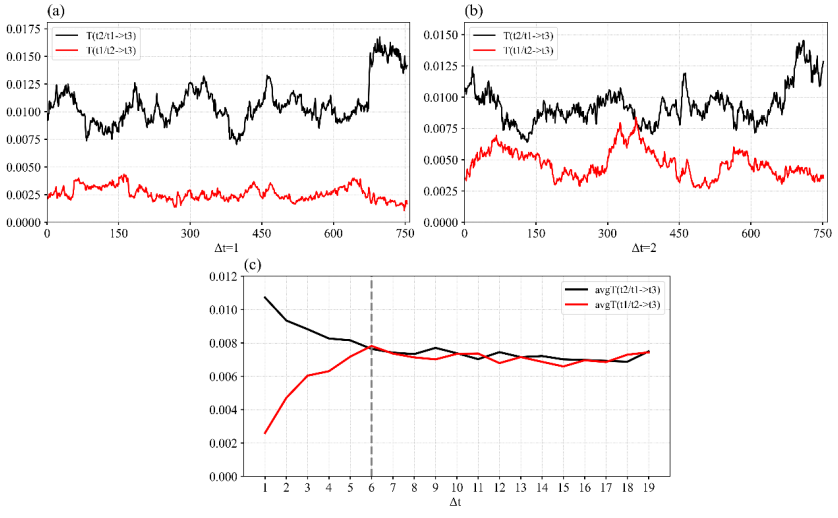

Figure 4: (a) Lagged transfer entropy of SST, (b) (△t =1, sample length=100), and (c) lagged transfer entropy of SST with sampling interval: △t=1–20.

https://doi.org/10.5194/egusphere-2024-2181
Preprint. Discussion started: 19 July 2024

The SST sequence was partitioned into lagged subsequences (with a sample size of 100), each consisting of three sequences (X, Y, and Z) corresponding to sampling time points t1, t2, and t3. For the third sequence group, the sampling interval was Δt=t3-t2=t2-t1=1–20. According to definition of transfer entropy, the transfer entropy T(t1/t2→t3) and T(t2/t1→t3) values can be obtained. Based on Fig. S1, the two transfer entropy values for each sample group were obtained (see Fig. 4a and 4b), and their areas were represented as two numerical values, yielding a transfer entropy area sequence for $\triangle$t=1–20 as shown in Fig. 4c.

When ignoring the absolute values of the transfer entropy, an interesting phenomenon was observed between the two transfer entropy values. The time interval between t2 and t3 was always smaller than that between t1 and t3, i.e., t3-t2=t2-t1=1–20, and t3-t1 was twice that of the former. Before $\triangle$t<7, the contribution of sampling points t2 to t3 gradually decreased under condition t1, whereas the contribution of sampling points t1 to t3 gradually increased under condition t2. Both converged to a constant value at $\triangle$t=6. It is clear that the blue line initially starts above the red line, as the time distance between t2 and t3 is always less than that between the latter, indicating that the contribution of t2 to t3 (or the percentage of t3) is higher than that of the former. After $\triangle$t>6, the contribution of t2 to t3 decreases to a basic constant value. Corresponding to t3-t1=$\triangle$t=2, 4, 6, 8, 10, 12, the contribution of t1 to t3 gradually increases and maintains the same state as the blue line. As the time span from t1 to t3 increases, the contribution of t1, which is further away from t3, increases. According to the definition of the transfer entropy calculation formula, this phenomenon occurs because the influence of t2 as a precondition decreases as the time span increases, resulting in a reduced impact on t3. However, although the influence of t1 as the driving component also decreases, its rate of decrease is slower than that of t2. This relationship resembles the combination of numerator and denominator relationships in conditional probability. Therefore, the contribution of t1 to t3, as indicated by the value of the transfer entropy based on t2, inevitably increases.

From the perspective of constructing the MKF, the two transfer entropies as mutual conditions indicate that the scale of memory changes occurs within 6–12 months. After 12 months, the memory remains almost unchanged. The changing state also indicates the existence of memory relationships between the sampling points. Based on this, the 6-month retrospective time scale can be used as the memory scale to construct the MKF, indicating that SST has relatively reliable inertial memory within 6 months.

3.3 Correlation coefficient

https://doi.org/10.5194/egusphere-2024-2181
Preprint. Discussion started: 19 July 2024

The correlation coefficient is a descriptive statistic measuring the degree to which changes in one variable correspond to those in another. According to its definition, the correlation coefficient only reflects synchronous changes between two variables and does not indicate causality between them. This does not affect its use in analyzing the problem of relationship memory. Following the lagged calculation scheme described above, the sliding correlation coefficient between the time series of the two sampling points was calculated with a subsequence length of 100. Figure 5 illustrates the variation in the average value of the lagged total sliding correlation coefficient.

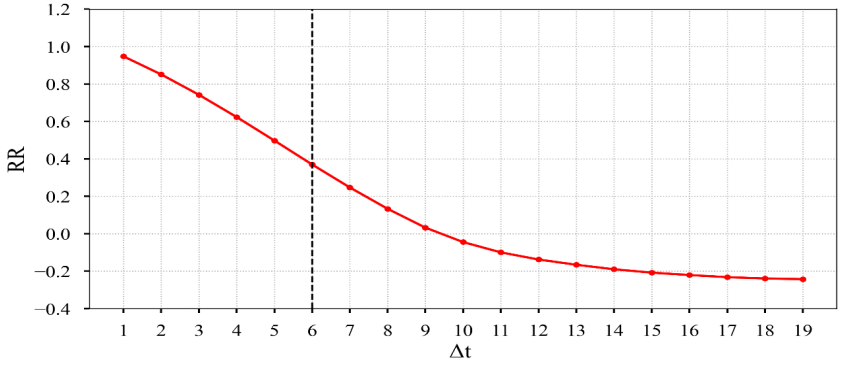

Figure 5: Lagged correlation coefficients.

As shown in Fig. 5, as the time between sampling points increases, the correlation coefficient gradually decreases and becomes negative after a gap of approximately 10 months. If the confidence level for the correlation coefficient is set at 0.01, the corresponding correlation coefficient is approximately 0.39, with a lagged time span of approximately 6 months. With a further increase in the time span, the correlation is lost near 9.5 months, and thereafter, the correlation fluctuates randomly. It is evident that this inertial memory length aligns closely with the transfer entropy results. Therefore, when constructing the MKF, the maximum number of initial values considered was set to seven (including the current initial value). Consequently, compared to the previous method of randomly selecting the past 24 initial values, this initial value scale can substantially narrow the range of numerical solutions searched in evolutionary modeling, thereby potentially improving the modeling efficiency.

https://doi.org/10.5194/egusphere-2024-2181
Preprint. Discussion started: 19 July 2024

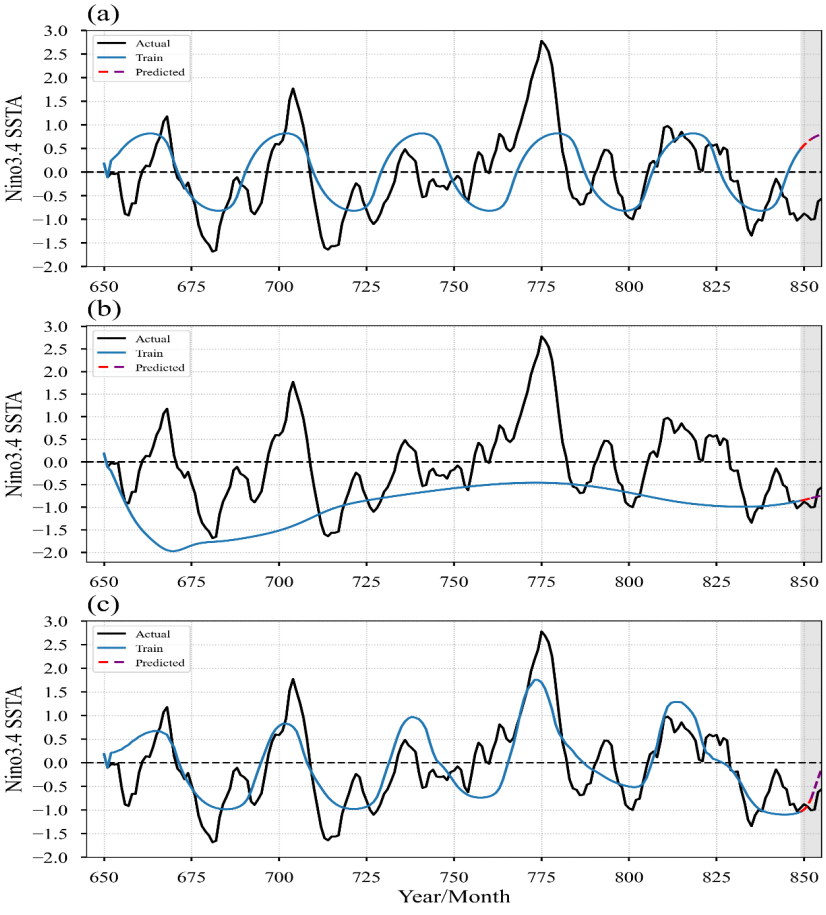

Figure 6: (a) Integral curve of inertial MKF, (b) integral curve of high-frequency disturbance component, and (c) integral curve of ODE-MKF based on inertial memory kernel function.

Through the characterization of memory using the tanh function of the inertial switch, the individual integral curve of the kernel function, as shown in Fig. 6a, describes relatively regular cyclical characteristics. Meanwhile, the high-frequency component ff, composed of retrospective value vectors and trigonometric functions, also exhibits certain nonlinear characteristics, as reflected in its individual integral curve in Fig. 6b, indicating a certain trend change. The ODE-MKF combines the advantages of both, further enhancing the understanding of oscillations in SST evolution details, with specific fitting parameters, including correlation coefficients and mean square errors. The test interval parameters are specified. Compared to the aforementioned cyclical memory, the ODE-MKF still exhibits considerable differences,

https://doi.org/10.5194/egusphere-2024-2181
Preprint. Discussion started: 19 July 2024

with the former showing more frequent small random fluctuations and the latter reflecting smoother cyclical patterns, as shown in Fig. 6c. Both demonstrated good predictive capabilities for trends.

4 Discussion and Conclusion

We used wavelet analysis to detect both periodic and non-periodic features in SST data and constructed periodic MKFs and inertial MKFs to record the two types of motion in the system. The results provide important novel insights into the temporal dynamics of complex systems. Researchers have estimated and evaluated the link between observable variables and model parameters using evolutionary algorithms, transfer entropy and correlation coefficients, which aids in the selection and improvement of models. Moreover, focused modeling with the backtracking of multiple initial values provides a strong foundation for improving the accuracy and dependability of differential equation models and overcomes the inverse problem of complex and nonlinear systems more efficiently. Using these methods to construct and solve the periodic and inertial MKFs for ENSO, we obtained better ENSO predictions.

Using multiple initial values to extends the single initial value inverse problem to backtracking multiple initial values and utilizing more historical information from the time series. By incorporating evolutionary algorithms into the model with improved equations, the model parameters and initial conditions were estimated. Improving the operation of equations and using evolutionary algorithms, researchers can quickly explore the solution space and find the configurations that best fit the observed data. The model parameters can be improved through this iterative optimization process such that they match the underlying dynamics of the system more closely, additionally, improves the precision and dependability of differential equation models (Chen et al., 2022).

From these findings, the temporal dynamics of complex systems can be better understood by examining the short space–time memory patterns. Two separate techniques for modeling temporal dependencies: inertial memory, which is characterized by the persistence of prior states for a specific length. This tool can use to quantification the ENSO interannual Extended cyclo-stationarity quasi-cycles and consider the possible ENSO memory (Gaucherel, 2010). Periodic memory, which is reflected by repeated cycles in the states of the system (Lustig et al., 2017). The variability of the Niño 1-2 and Niño 3 has large component of long-memory behavior associated with the quasi-biennial and the semi-annual frequency. This is particularly true when analyzing targeted modeling, which involves the retracing of several initial values.

https://doi.org/10.5194/egusphere-2024-2181
Preprint. Discussion started: 19 July 2024

Understanding the characteristics of periodic and inertial memory is essential for understanding the behavior of a system in the long run. The selection of suitable MKFs for modeling can be greatly aided by examining SST memory patterns. Prevalent cycles in SST data were identified using wavelet analysis, which directs the creation of MKFs specifically designed to capture the memory properties of a system (Brown and Garcia, 2021). Characteristic factors, such as inertial motion and periodic cycles, were identified to guide the creation of MKFS that efficiently capture temporal dependencies in the observed data.

To represent the memory dynamics of the system over time, inertial MKFs are essential for capturing the system's inertial motion (Wang and Zhang, 2021). To develop the inertial MKFs, the magnitude of memory changes in the system was ascertained by examining the lagged transfer entropy. Researchers can increase the fidelity of differential equation models to capture the inertial memory properties of a system by including inertial MKFs in the modeling framework. As a gauge of the linear link between variables, the correlation coefficient sheds light on the synchronous changes that occur between two variables (Johnson and Smith, 2019). The correlation coefficient makes it easier to evaluate the link between the observed data and model parameters in the context of focused modeling. The choice of suitable model structures, inertial memory ranges and parameterizations is guided by the observed correlations between variables, which improves the precision of the differential equation models.

This study highlights the advantage of using focused modeling with backtracked multiple initial values to understand the temporal dynamics of complex systems. Researchers can advance state-of-the-art modeling approaches and obtain deeper insights into the dynamics of complex systems by examining SST memory patterns, utilizing correlation coefficients, combining evolutionary algorithms, and applying inertial MKFS.

Acknowledgments.

We are grateful to the public data websites for providing the data sets used in this study at no cost. This research was funded by the National Natural Science Foundation of China (Grant No. 42075051 and No.42205023).

Code availability

The code supporting the results of this study can be obtained from the corresponding authors according to reasonable requirements.

https://doi.org/10.5194/egusphere-2024-2181
Preprint. Discussion started: 19 July 2024

Data Availability

The original contributions presented in the study are included in the article. Further enquiries can be directed to the corresponding authors.

Author contributions

SW: Conceptualization; Methodology; Writing–original draft; HL: Formal analysis; Writing–original draft; LZ: Investigation; Supervision; XZ: Investigation; Supervision; SX: Investigation; Supervision; MQ: Investigation; Supervision; YC: Investigation; Supervision. QM: Investigation; Supervision; Writing–original draft.

Competing interests

The contact author has declared that none of the authors has any competing interests.

REFERENCES

Alizadeh, O.: Advances and challenges in climate modelling, Clim. Change, 170, 18, https://doi.org/10.1007/s10584-021-03298-4, 2022.

Chen, D., Cane, M. A., Kaplan, A., Zebiak, S. E., and Huang, D.: Predictability of El Niño over the past 148 years, Nature, 428, 733–736, https://doi.org/10.1038/nature02439, 2024.

Chen, N., Fang, X., and Yu, J.-Y.: A multiscale model for El Niño complexity, npj Clim. Atmos. Sci., 5, 16–29, https://doi.org/10.1038/s41612-022-00241-x, 2022.

Chen, X., Xia, J., and Xu, Q.: Differential Hydrological Grey Model (DHGM) with self-memory function and its application to flood forecasting, Sci. China Ser. E-Technol. Sci., 52, 1039–1049, https://doi.org/10.1007/s11431-008-0320-5, 2009.

Dong, W., Chou, J., and Feng, G.: Progress in the study of retrospective numerical scheme and the climate prediction, Acta. Mech. Sin., 20, 455–464, https://doi.org/10.1007/BF02484267, 2004.

Drosdowsky, W.: Statistical prediction of ENSO (Nino 3) using sub‐surface temperature data, Geophys. Res. Lett., 33, 2005GL024866, https://doi.org/10.1029/2005GL024866, 2006.

Eyring, V., Cox, P. M., Flato, G. M., Gleckler, P. J., Abramowitz, G., Caldwell, P., Collins, W. D., Gier, B. K., Hall, A. D., Hoffman, F. M., et al.: Taking climate model evaluation to the next level, Nat. Clim. Change, 9, 102–110, https://doi.org/10.1038/s41558-018-0355-y, 2019.

https://doi.org/10.5194/egusphere-2024-2181
Preprint. Discussion started: 19 July 2024

Feng, G., Cao, H., Gao, X., Dong, W., and Chou, J.: Prediction of Precipitation during Summer Monsoon with Self-memorial Model, Adv. Atmos. Sci., 18, 701–709, https://doi.org/10.1007/BF03403495, 2001.

Feng, G., and Dong, W.: Evaluation of the applicability of a retrospective scheme based on comparison with several difference schemes, Chin. Phys., 12, 1076, https://doi.org/10.1088/1009-1963/12/10/307, 2003.

Feng, G., Yang, J., Zhi, R., Zhao, J., Gong, Z., Zheng, Z., Xiong, K., Qiao, S., Yan, Z., Wu, Y., et al.: Improved prediction model for flood-season rainfall based on a nonlinear dynamics-statistic combined method, Chaos, Solitons Fractals, 140, 110160, https://doi.org/10.1016/j.chaos.2020.110160, 2020.

Feng, X., Ling, X., Zheng, H., Chen, Z., and Xu, Y.: Adaptive Multi-Kernel SVM With Spatial–Temporal Correlation for Short-Term Traffic Flow Prediction, IEEE Trans. Intell. Transp. Syst., 20, 2001–2013, https://doi.org/10.1109/TITS.2018.2854913, 2019.

Gaucherel, C.: Analysis of ENSO interannual oscillations using non‐stationary quasi‐periodic statistics: A study of ENSO memory, Int. J. Climatol., 30, 926–934, https://doi.org/10.1002/joc.1937, 2010.

Guan, Y., Zheng, F., Zhang, P., and Qin, C.: Spatial and temporal changes of meteorological disasters in China during 1950–2013, Nat. Hazards, 75, 2607–2623, https://doi.org/10.1007/s11069-014-1446-3, 2015.

He, W., Feng, G., Wu, Q., He, T., Wan, S., and Chou, J.: A new method for abrupt dynamic change detection of correlated time series, Int. J. Climatol., 32, 1604–1614, https://doi.org/10.1002/joc.2367, 2012.

Hwang, J., Choi, J., Choi, H., Lee, K., Lee, D., and Park, N.: Climate Modeling with Neural Diffusion Equations, 2021 IEEE International Conference on Data Mining (ICDM), 230-239, https://doi.org/10.48550/arXiv.2111.06011, 2021.

Kjellström, E., Boberg, F., Castro, M., Christensen, J. H., Nikulin, G., and Sánchez, E.: Daily and monthly temperature and precipitation statistics as performance indicators for regional climate models, Clim. Res., 44, 135–150, https://doi.org/10.3354/cr00932, 2010.

Lima, C. H. R., Lall, U., Jebara, T., and Barnston, A. G.: Statistical Prediction of ENSO from Subsurface Sea Temperature Using a Nonlinear Dimensionality Reduction, J. Clim., 22, 4501–4519, https://doi.org/10.1175/2009JCLI2524.1, 2009.

Lu, W., Atkinson, D. E., and Newlands, N. K.: ENSO climate risk: predicting crop yield variability and coherence using cluster-based PCA, Model. Earth Syst. Environ., 3, 1343–1359, https://doi.org/10.1007/s40808-017-0382-0, 2017.

https://doi.org/10.5194/egusphere-2024-2181
Preprint. Discussion started: 19 July 2024

Lustig, A., Charlot, P., and Marimoutou, V.: The memory of ENSO revisited by a 2-factor Gegenbauer process, Int. J. Climatol., 37, 2295–2303, https://doi.org/10.1002/joc.4843, 2017.

Ma, Q., Sun, Y., Wan, S., Gu, Y., Bai, Y., and Mu, J.: An ENSO Prediction Model Based on Backtracking Multiple Initial Values: Ordinary Differential Equations–Memory Kernel Function, Remote Sens., 15, 3767, https://doi.org/10.3390/rs15153767, 2023.

Masson, D., and Knutti, R.: Climate model genealogy. Geophys. Res. Lett., 38, https://doi.org/10.1029/2011GL046864, 2011.

Mirikitani, D. T., and Nikolaev, N.: Recursive Bayesian Recurrent Neural Networks for Time-Series Modeling, IEEE Trans. Neural Networks, 21, 262–274, https://doi.org/10.1109/TNN.2009.2036174, 2010.

Mittal, A. K., Singh, U. P., Tiwari, A., Dwivedi, S., Joshi, M. K., and Tripathi, K. C.: Short-term predictions by statistical methods in regions of varying dynamical error growth in a chaotic system, Meteorol. Atmos. Phys., 127, 457–465, https://doi.org/10.1007/s00703-015-0375-3, 2015.

Olivetti, L., and Messori, G.: Advances and prospects of deep learning for medium-range extreme weather forecasting, Geosci. Model Dev., 17, 2347–2358, https://doi.org/10.5194/gmd-17-2347-2024, 2024.

Palmer, T. N.: A nonlinear dynamical perspective on model error: A proposal for non ‐ local stochastic ‐ dynamic parametrization in weather and climate prediction models, Q. J. R. Meteorol. Soc., 127, 279–304, https://doi.org/10.1002/qj.49712757202, 2001.

Reynolds, R. W., and Smith, T. M.: Improved Global Sea Surface Temperature Analyses Using Optimum Interpolation, J. Clim., 7, 929–948, https://doi.org/10.1175/1520-0442(1994)007<0929:IGSSTA>2.0.CO;2, 1994.

Sedki, A., Ouazar, D., and Mazoudi, E. E.: Evolving neural network using real coded genetic algorithm for daily rainfall-runoff forecasting, Expert Syst. Appl., 36, 4523–4527, https://doi.org/10.1016/j.eswa.2008.05.024, 2009.

Sunyer, M. A., Madsen, H., and Ang, P. H.: A comparison of different regional climate models and statistical downscaling methods for extreme rainfall estimation under climate change, Atmos. Res., 103, 119–128, https://doi.org/10.1016/j.atmosres.2011.06.011, 2012.

Tian, F., Zheng, Y., Zhang, T., Zhang, X., Mao, D., Sun, J., and Zhao, S.: Statistical characteristics of environmental parameters for warm season short-duration heavy rainfall

https://doi.org/10.5194/egusphere-2024-2181
Preprint. Discussion started: 19 July 2024

over central and eastern China, J. Meteorol. Res, 29, 370–384, https://doi.org/10.1007/s13351-014-4119-y, 2015.

Usman, A.: Integrated disaster risk management in Indian environment: Prediction, prevention and preparedness, 2017 IEEE Global Humanitarian Technology Conference (GHTC), 1–6, https://doi.org/10.1109/GHTC.2017.8239246, 2017.

Wan, S., He, W., Wang, L., Jiang, W., and Zhang, W.: Evolutionary modeling-based approach for model errors correction, Nonlin. Processes Geophys., 19, 439–447, https://doi.org/10.5194/npg-19-439-2012, 2012.

Wei, F.: Physical basis of short-term climate prediction in China and short-term climate objective prediction methods (in Chinese), J. Appl. Meteor. Sci., 22, 1–11, http://qikan.camscma.cn/jamsweb/article/id/20110101, 2011.

Wu, J., Fu, Y., Zhang, J., and Li, N.: Meteorological disaster trend analysis in china: 1949-2013 (in Chinese), J. Nat. Resour., 29, 1520–1530, https://doi.org/10.11849/zrzyxb.2014.09.007, 2014.

Zhang, P., Jia, Y., Gao, J., Song, W., and Leung, H.: Short-term rainfall forecasting using multi-layer perceptron, IEEE Trans. on Big Data, 6, 93–106, https://doi.org/10.1109/TBDATA.2018.2871151, 2018.